

Evaluation and Improvements to a Mechanical Engineering Capstone Designed Autoclave
System for Use in High Temperature Aqueous Environments

A Thesis

Presented in Partial Fulfillment of the Requirements for the

Degree of Master of Science

with a

Major in Mechanical Engineering

in the

College of Graduate Studies

University of Idaho

by

Colin J. Burkhalter

Major Professor: Robert Stephens, Ph.D.

Committee Members: Gabriel Potirniche, Ph.D.; Krishnan Raja, Ph.D.

Department Chair: Gabriel Potirniche, Ph.D.

August 2020

Authorization to Submit Thesis

Abstract

Servo-hydraulic load frames have been used to perform fatigue testing for decades. Additions to these frames, such as high temperature furnaces and torsional stressing, have allowed for increased research opportunities. An area of additional needed fatigue research is the nuclear industry. Crack growth analysis in an aqueous reactor environment with high temperature and pressure is needed. Specimens in this environment provide fatigue data in a corrosive environment when subjected to these conditions for long tests. To gather this data, a new experimental system is required. One such system was designed by a senior capstone group at the University of Idaho. The system was developed from a modified autoclave with a servo-hydraulic frame attached to it. The system was designed to be attached to a fluid control panel that would circulate pressurized water into the autoclave. This system could be heated and would fully simulate a reactor environment. Several issues emerged in the building of this system. The control and functionality was limited, causing the need for future improvements. Improving the cooling jacket, seals, fluid control, and data collection process was performed. Several iterations of these processes were attempted. Preliminary testing of these new devices was performed to show the progress and results. Data was collected in both air and water as the working fluid filling the autoclave chamber. Several heated and pressurized tests were performed as well. Problems were encountered upon several stages of the initial testing. While promising results were gathered, future improvements are still needed. Safety features as well as additional system cooling will need to be applied. Once completed, this system can perform fatigue testing in a heated and pressurized aqueous environment simulating that of a reactor.

Acknowledgments

Table of Contents

AUTHORIZATION TO SUBMIT THESIS	II
ABSTRACT	III
ACKNOWLEDGMENTS	IV
TABLE OF CONTENTS	V
LIST OF FIGURES	VII
LIST OF TABLES	IX
NOMENCLATURE	X
1. INTRODUCTION	1
2. LITERATURE REVIEW	2
2.1 GENERATION IV REACTORS	2
2.2 FRACTURE MECHANICS AND EQUATIONS	3
2.3 FATIGUE CRACK GROWTH	7
2.4 ALLOY 709	8
2.5 STRESS CORROSION CRACKING	9
3. SYSTEM SETUP	11
3.1 PREVIOUS SYSTEM	11
3.1.1 Autoclave Sealing	12
3.1.2 Cooling Jacket	13
3.1.3 Control System	14
3.1.4 Closed Water Loop	15
3.2 IMPROVEMENTS/CHANGES	15
3.2.1 Connection of the Water Loop System	15
3.2.2 Cooling Jacket	18
3.2.3 Seals	21
3.2.4 DCPD Wire Ports	23
3.2.5 Fluid Controls	25
3.2.6 Controls and Data Recording	26
3.2.7 Gaskets	27
4. EXPERIMENTAL DETAILS	30
4.1 MATERIAL AND SPECIMEN DETAILS	30
4.2 EXPERIMENTAL PROCEDURE	31
4.2.1 Precracking	31
4.2.2 DCPD Measurement Technique	32
4.2.3 Setup in Autoclave	33
4.2.4 Breaking the Specimen	34
4.3 DATA COLLECTION	34
4.3.1 Software Analytics	34
4.3.2 Microscopy	34
5. RESULTS	36
5.1 COMPARING AUTOCLAVE TO ADDITIONAL LOAD FRAMES	36
5.2 DATA COLLECTION IN PURE WATER	37

5.3 DATA COLLECTION IN HEATED AND PRESSURIZED WATER	39
5.4 TOTAL TEST COMPARISON.....	40
6. CONCLUSIONS.....	41
6.1 AUTOCLAVE FATIGUE PERFORMANCE	41
6.2 COLLECTING DCPD DATA IN WATER	41
6.3 COLLECTING DCPD DATA IN ABOVE BOILING TEMPERATURE WATER	41
7. RECOMMENDATIONS.....	42
7.1 SEALING AND COOLING.....	42
7.2 NOTIFICATION SYSTEM	44
7.3 MAINTENANCE.....	45
REFERENCES	47
APPENDICES	48

List of Figures

FIGURE 2.1: MODEL OF A POOL TYPE SODIUM-COOLED FAST REACTOR

FIGURE 2.2: MODES OF CRACK DISPLACEMENT

FIGURE 2.3: REGIONS OF CRACK GROWTH AND PARIS CURVE

FIGURE 2.4: MEAN STRESS RATIO EFFECT ON CRACK GROWTH RATE

FIGURE 2.5: MATERIAL CHARACTERISTICS OF GEN IV REACTOR CANDIDATE MATERIALS

FIGURE 2.6 H₂ FUGACITY EFFECTS ON CRACK GROWTH RATES

FIGURE 2.7: SCC EFFECTS UPON A TEST SPECIMEN

FIGURE 3.1: AUTOCLAVE METAL RING SEAL

FIGURE 3.2: ORIGINAL SEALS USED IN THE COOLING JACKET

FIGURE 3.3: ORIGINAL COOLING JACKET WITH WATER LINE CONNECTIONS

FIGURE 3.4: HIGH PRESSURE PUMP USED BY THE CWL

FIGURE 3.5: WATER RESERVOIR FOR CWL

FIGURE 3.6: ORIENTATION OF FLOW VALVES TO OPERATE CWL

FIGURE 3.7: FAILED HIGH PRESSURE SEAL

FIGURE 3.8: COOLING JACKET WITH COILS ATTACHED

FIGURE 3.9: TEMPERATURE PROFILES DURING COOLING JACKET TESTING

FIGURE 3.10: V-RING SEAL SET

FIGURE 3.11: WFS WIRE PORTS SCHEMATICS

FIGURE 3.12: AIR COMPRESSOR AND GAUGE ATTACHMENT

FIGURE 3.13: TEMPERATURE CONTROLLER AND MONITOR

FIGURE 3.14: LOWER GASKET ATTACHED TO COOLING JACKET

FIGURE 3.15: DAMAGE TO AUTOCLAVE METAL SEAL

FIGURE 4.1: C(T) SPECIMEN DIMENSIONS IN ACCORDANCE WITH ASTM E-647

FIGURE 4.2: C(T) SPECIMEN WIRING SCHEMATIC

FIGURE 4.3: BROKEN SPECIMEN SURFACE AND CRITICAL CRACK LENGTH POSITIONS

FIGURE 5.1: FCG TEST DATA COMPARISON BETWEEN THE ORIGINAL LOAD FRAME AND THE AUTOCLAVE

FIGURE 5.2: RT COMPARISON OF FCG TEST IN AIR AND WATER

FIGURE 5.3: SHIFTING DUE TO APPLIED FRICTIONAL FORCE

FIGURE 5.4: ALL TESTS COMPLETED DURING RESEARCH

FIGURE 7.1: POSSIBLE COOLING JACKET MODIFICATIONS

List of Tables

TABLE 3.1: V-RING SEAL SET ADDITIONAL COMPRESSION TESTING

TABLE 4.1: MATERIAL COMPOSITION BY % MASS

Nomenclature

a	crack length
w	width
C(T)	compact tension specimen
FCG	fatigue crack growth
da/dN	fatigue crack growth rate
DCPD	direct current potential drop
E	elastic modulus
K	stress intensity
K_{min}	minimum stress intensity in a cycle
K_{max}	maximum stress intensity in a cycle
ΔK	stress intensity range
N	number of applied cycles
SFR	sodium fast reactor
RT	room temperature
CWL	closed water loop
O ₂	oxygen
SHCS	socket head cap screw
BWR	boiling water reactor
EDM	electronic discharge machining
ASTM	American Society for Testing and Materials
CFCG	creep fatigue crack growth

1. Introduction

Servo-hydraulic tensile testing machines have been used for decades to perform fatigue testing research upon a myriad of materials and specimens. These tests have improved the designs of numerous structures and equipment increasing the lifespan of these components. Several adaptations of these frames such as encased furnaces and torsional stress applications have allowed for increased research capabilities. The ability to test in a new environment provides critical data to many fields of work. One such field with needed fatigue data is the nuclear industry. These reactors experience extreme working conditions of pressure and temperature. To perform various material characteristic testing, new experimental systems are needed. An autoclave test frame was designed by a capstone team at the University of Idaho for this purpose. The goal of this modified autoclave was to perform several different tests including SCC (stress corrosion cracking), slow strain rate, and FCG (fatigue crack growth) while in a heated and pressurized aqueous environment simulating reactor settings. For the existing system to achieve this goal, several improvements are needed. While improving the functionality of the autoclave and collecting data in several different tests, there are still changes needed to be made in the future.

2. Literature Review

2.1 Generation IV Reactors

The rising need for more power and efficiency in the energy department has created the stage for a new generation of power. The nuclear industry is one field that is undergoing changes to meet this demand. Generation IV reactors are being designed to supplant the current generation of reactors powering our country (3). Three new reactor concepts have been developed and are classified by the coolant used in the system. The main concept under consideration is the Sodium Fast Reactor (SFR) which uses a liquid-metal sodium coolant solution (1). The new SFR coolant system is 100 times more effective than traditional water usage and is still compatible with the previous system piping techniques (2). This system creates a much more efficient reactor, as well as one that is easier to manage and control in the event of damage to the system.

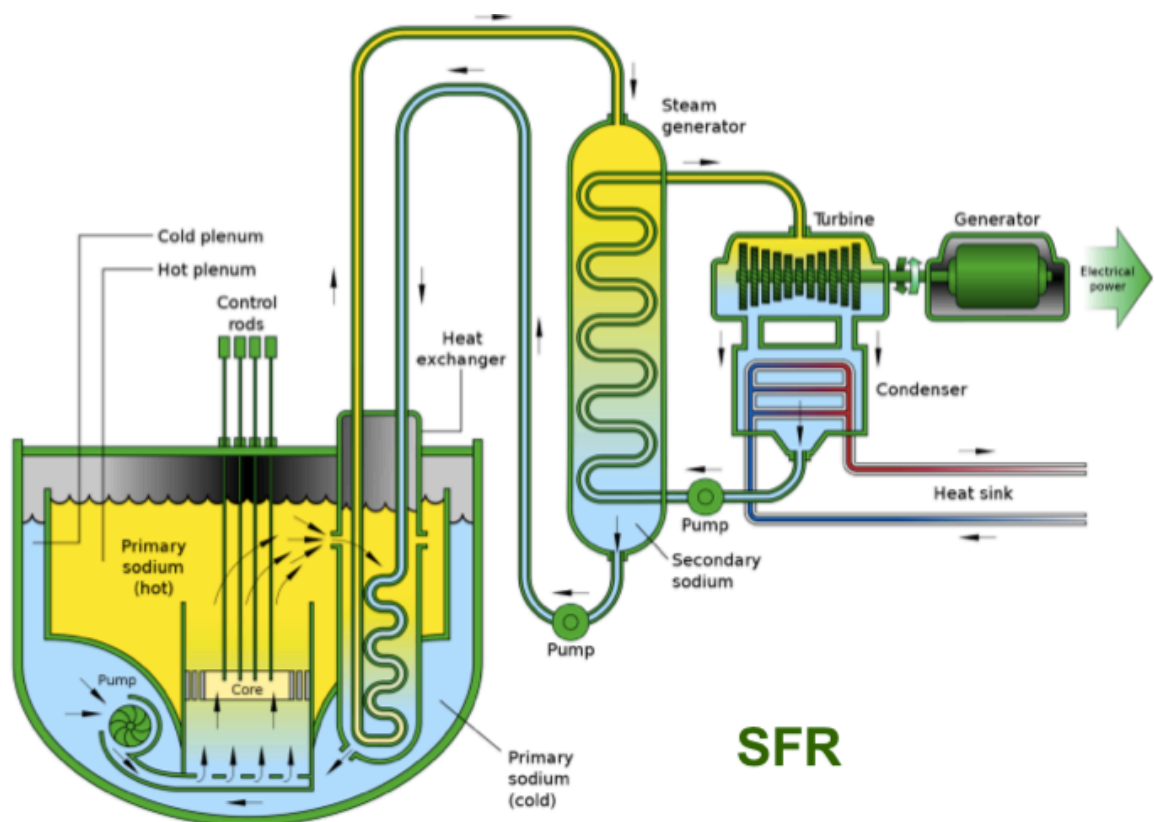


Figure 2.1: Model of a Pool type sodium-cooled fast reactor (1)

Several challenges exist to the development of this future generation of reactors including: resistance to irradiation damage, creep resistance at high temperature, and corrosion resistance (3). The operating temperature will be greater than 500°C in the core, creating an environment that amplifies the possible damage mentioned above (1). The largest safety concern is the sodium coolant being reactive with both water and air, lending to the need for a leak-proof system (1). Materials used in the construction of these reactors must combat these problems. The operating life of a generation IV reactor will require 60+ years of service under various loading parameters. High levels of corrosion and heat transfer occur in the daily usage of this system. The need for a material with high creep resistance, strength and ductility is paramount to construct this new type of reactor (3). One such attractive candidate material is an austenitic stainless steel Alloy 709. This material has shown advanced creep and corrosion resistance. Alloy 709 is compatible with sodium and is under extensive testing to determine its effectiveness as a replacement for previously used 316 alloys (4).

2.2 Fracture Mechanics and Equations

Fracture mechanics is described as, “a method of characterizing the fracture and the fatigue behavior of sharply notched structural members.” This method of determining behavior uses a mathematical calculation relating the crack length to the load applied for a given specimen geometry (5). The stress intensity factor, K , is the component commonly used to characterize a crack in a component or structure. Development of this model was made by Alan Griffith in the 1920’s. He showed that the stress imparted upon an object is related to the square root of the crack length along with certain material properties. George Irwin later improved upon this method by relating the stress intensity factor by use of Young’s modulus and Poisson’s ratio. (6).

Fatigue as defined by ASTM (American Society for Testing and Materials) is: The process of progressive localized permanent structural change occurring in a material subjected to conditions that produce fluctuating stresses and strains at some point or points and that may culminate in cracks or complete fracture after enough fluctuations (6). Several parts of this definition help clearly illustrate what and how fatigue failures occur.

Fatigue crack growth occurs over lengths of time during which cyclic loading occurs which can vary in length from a few hundred to multiple millions of cycles. This constant stress application causes localized slips of atomic planes to occur within the metal at the surface. These stresses over time eventually cause a crack to form. Microscopic cracks usually nucleate along the maximum shear stress planes. Cracks will continue to nucleate and grow inside these grain boundaries along this plane until enough dislocations have occurred to create a fatigue crack. These combined cracks will eventually coalesce and continue to grow along the maximum tensile stress plane

Fundamentally, fracture mechanics is used to solve for a stress intensity at a point in an object under fatigue in the presence of a crack. To do this the definition of the crack movement in the specimen is needed. Three individual crack displacement modes have been defined to analyze the stress intensity in each case. The three modes operate in normal tensile loading, direct shear, and out of plane shear along the crack axis (5).

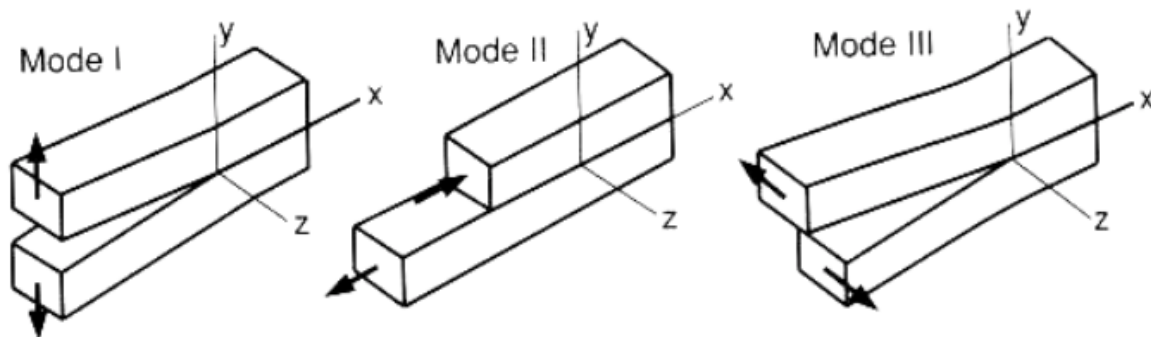


Figure 2.2: Modes of Crack Displacement

Mode 1 is the most used and applicable displacement mode. For mode 1 displacement, Equation 1 in the form of

$$K = Y * S * \sqrt{a} \quad (1)$$

is used to find the stress intensity where S is stress in the specimen and a is the crack length (6). The geometry constant, Y , is dimensionless and is determined by the specimen

geometry and how the crack is growing in the specimen. Y is a function of both crack length, a , and width, w , and is commonly written as

$$Y = F\left(\frac{a}{w}\right) \quad (2)$$

The function $F\left(\frac{a}{w}\right)$ for the C(T) specimen geometry used in this study is given as:

$$F\left(\frac{a}{w}\right) = \frac{(2 + \alpha)}{(1 - \alpha)^2} (0.886 + 4.64\alpha - 13.32\alpha^2 + 14.72\alpha^3 - 5.6\alpha^4) \quad (3)$$

where $\alpha = a/w$. Equation 3 is per the American Society for Testing and Materials standard E-647 for the C(T) specimen and accounts for the axial and bending components applied to the specimen as the crack length increases (7).

During a fatigue test, the specimen can experience a range of stresses applying multiple stress intensities. This range is called the stress intensity range or more commonly ΔK . Under constant amplitude loading this range has a set maximum and minimum being applied each cycle. This range is defined as

$$\Delta K = K_{max} - K_{min} \quad (4)$$

The largest value experienced is labeled as K_{max} and similarly the lowest value is K_{min} . In fracture mechanics, ΔK is an important value when analyzing how a crack grows in a specimen. The rate at which a crack grows is another important value analyzed when looking at FCG. This crack growth rate, da/dN , is the comparison of how fast the crack grows, Δa , to the number of cycles, ΔN , it takes to achieve that growth.

This rate is then paired with a ΔK for a given crack length to form the typical da/dN vs ΔK curve on log-log axis. This graph often takes on a sigmoidal shape which are segmented into three regions as shown in the figure above. Region 1 has much slower crack growth

rate since the stress intensity range is near the threshold value needed to advance the crack growth in the specimen. This leads to a long life and many cycles in region I while the crack slowly propagates. Region II is often estimated as a straight line and corresponds to the Paris equation in Equation 5

$$\frac{da}{dN} = A(\Delta K)^n \quad (5)$$

where n is the slope of the line and A is the coefficient found by extending the straight line to $\Delta K = 1 \text{ MPa}\sqrt{\text{m}}$. The crack in this region is less affected by microstructures and grows much more uniformly and quickly. Region III is where the crack growth rate approaches instability as the crack is growing very fast relative to the number of cycles needed to increase it. A small portion of the life span is spent in this region as fracture will occur shortly after entering it (6).

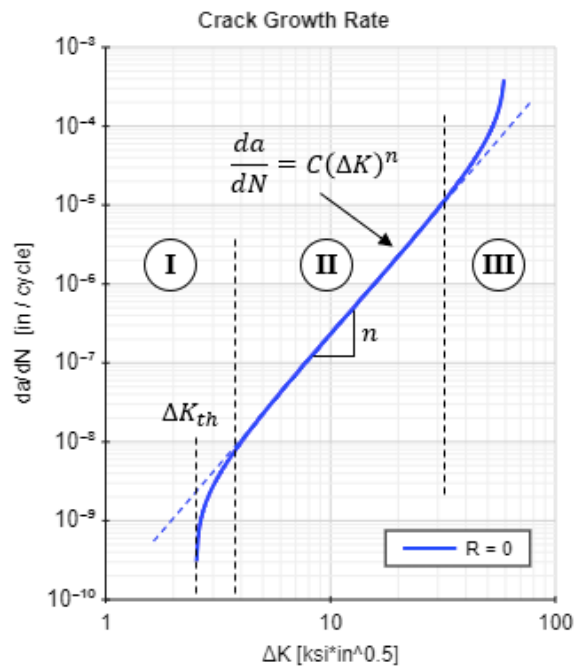


Figure 2.3: Regions of Crack Growth and Paris Curve

2.3 Fatigue Crack Growth

Fatigue tests in the laboratory are often performed on small specimens with simple geometries and through thickness cracks to document the crack growth. ASTM standards have been developed to regulate the analysis of these tests, most notably of which is ASTM Standard E647 (7). Two unique tests are performed on the specimen in order stimulate crack growth and propagate the crack to failure. The first test is what is called the “Fatigue Precrack”. This test is performed at a low ΔK at a notch on the specimen to stimulate a sharp crack tip for the crack to continue to grow (6). This precrack is grown out to a desirable length and ΔK for which the rest of the test proceed. The next section of the test is when the crack is grown under constant amplitude loading. As the cycles are applied, the crack propagates which increases the ΔK (6). As ΔK increases, so does da/dN leading to failure.

Fatigue testing of any compact tension specimen will use these two tests to calculate crack growth data for that metal. The main variable changed in testing of specimens is the mean stress applied to the specimen. The ratio of forces in a specimen is defined as R , as seen in equation 6

$$R = K_{min}/K_{max} = S_{min}/S_{max} \quad (6)$$

This is called the stress ratio where S represents stress in the specimen. As this ratio is increased at a constant crack growth rate, a lower ΔK is observed. This can be seen in Figure 2.4. Due to the higher stress per cycle the crack will grow at a quicker rate. This data shift can be used to determine how the material will perform when loaded under differing loading patterns.

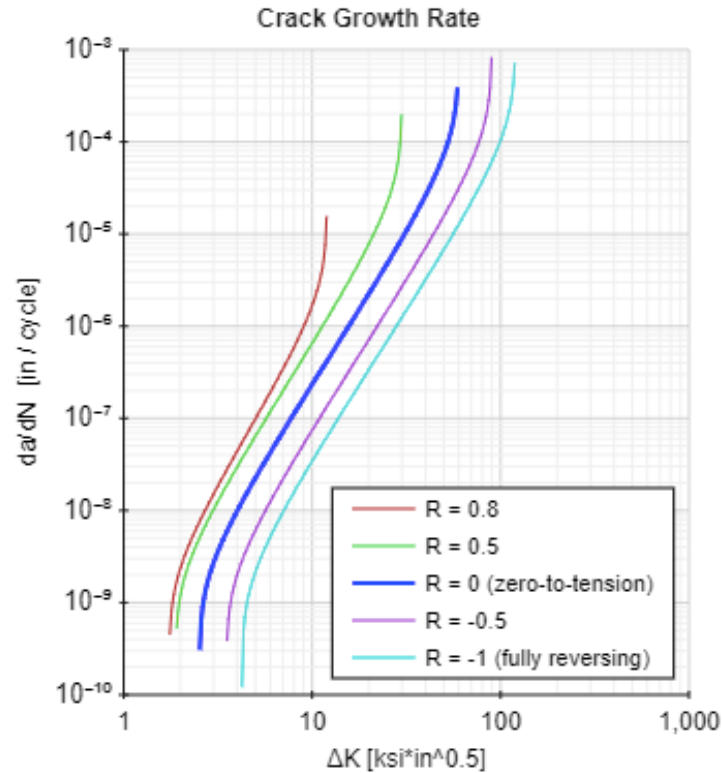


Figure 2.4: Mean Stress Ratio Effect on Crack Growth Rate

2.4 Alloy 709

As stated previously, Alloy 709 is a candidate for use in the new generation IV nuclear reactors. Materials in these structural conditions will be subjected to extreme environments. High temperature and corrosive circumstances will often be present in the reactor, leading to the need for a specialized material. Alloy 709 has shown excellent creep and corrosion resistance in previous testing as well as superb work hardening capability up to 650°C and ample ductility at all operating temperatures (8).

Alloy 709 is a 20Cr-25Ni advanced austenitic stainless steel developed as an improvement over existing advanced austenitic stainless steels (9). The high Ni content provides increased austenite stability. Most austenitic stainless steel alloys are corrosion and creep resistant by nature (10). These two characteristics make Alloy 709 a potential candidate for nuclear reactor building materials.

Thermal ageing and lifespan of the metal are characteristics that are of the utmost importance for a role such as this. Spending 60+ years in a reactor setting imparts

substantial damage upon a metal. Alloy 709 has been tested under several “aged metal” circumstances to determine any additional side effects imparted by service in a high temperature environment over time. Aging of metal at 650°C for 3-6 months simulates 25-50 years of life of the metal (10). Previous tests show that prolonged thermal ageing of the alloy did not appear to affect the crack growth rates under various FCG and CFCG (creep fatigue crack growth) loading conditions (11).

Many other materials of this nature have been tested to analyze their characteristics in essential categories. They include 316H and HT-UPS (High Temperature Ultrafine-Precipitate-Strengthened) stainless steels with multiple altered HT-UPS strains. As seen in the figure below, Alloy 709 possesses the best all-around property rankings in each category and is only surpassed in creep resistance by a HT-UPS strain (10). Overall the alloy shows the most promise to fulfill the expectations of the structural needs for the reactor.

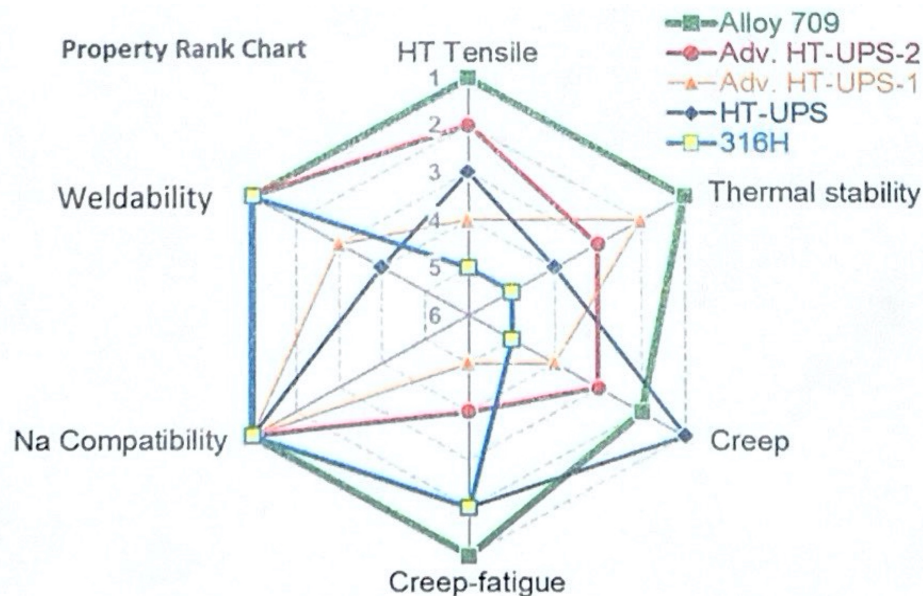


Figure 2.5: Material Characteristics of Gen IV Reactor Candidate Materials (10)

2.5 Stress Corrosion Cracking

Stress corrosion cracking, or SCC, is crack growth in a corrosive environment. This effect is often increased under high temperatures. SCC is a hazard most associated with materials working in water. As the working fluid in a nuclear reactor, purified water serves

as the catalyst for corrosion during the lifespan of the material. Water has been a working fluid in reactors since the beginnings of reactor development (13). Stainless steel alloys have been in use since the BWR (Boiling water reactor) as a counter to corrosion within the systems (14). SCC was seen substantially along weld lines limiting early systems to 5-10+ years of service life in certain members. Improvements in the purity of water and protective substance coverings have helped alleviate the growth and initiation of SCC in these sections to extend the length of use for materials to now 40+ years. As stated the goal of the Gen IV reactor is to reach 60+ years of service for all materials in use for the reactor, so extending use even further will require more innovation (13).

As Alloy 709 is a stainless-steel material with a high nickel composition percentage, it is susceptible to SCC in a water environment no matter the purity. A study to show the effect of H₂ fugacity on a similar metal of Alloy 600 was performed (14).

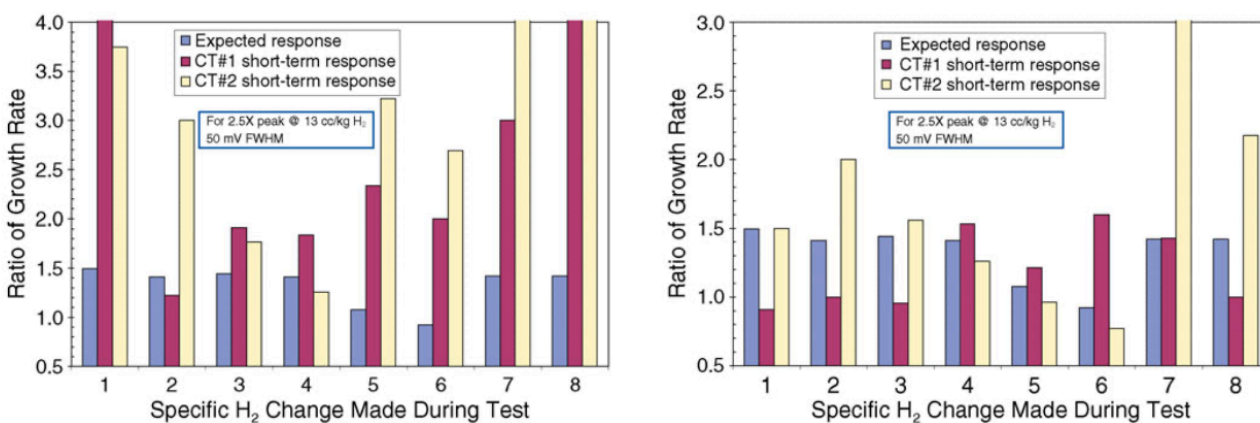


Figure 2.6 H₂ Fugacity Effects on Crack Growth Rates (14)

SCC and the strength at which it affects the specimen is dependent upon the specific H₂ change made during the test. Figure 2.6 shows the effects observed during these trials. As shown this nickel based alloy experienced a 2.5 – 3 times greater crack growth rate in the specimens than base values. These tests were performed in the representative pressurized water reactor chemistries currently employed in the industry (15).

It has been well established that sensitized austenitic stainless steels undergo intergranular stress corrosion cracking in pure water containing oxygen. Figure 2.7 shows how corrosion affects a metal specimen in a reactor's aqueous environment. There has been increasing evidence that the role of impurities in initiating and propagating stress corrosion cracks is very substantial (14). Numerous SCC tests were performed in corrosive environment on a similar metal of Alloy 304. The testing showed that at elevated temperatures of 280°C and greater the effect of the impurities became much stronger.

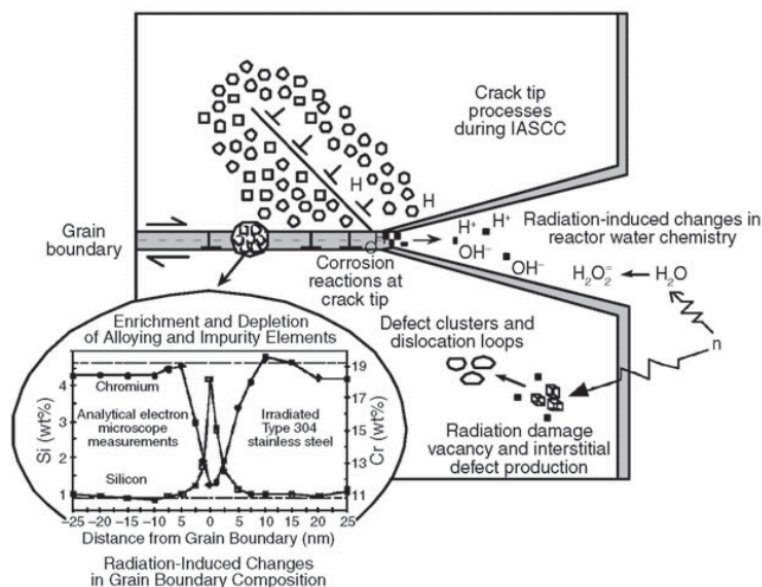


Figure 2.7: SCC Effects Upon a Test Specimen (16)

For example, at 1 ppm H_2SO_4 , failure was accelerated by about an order or magnitude and was not altered by reducing the oxygen concentration to 0.2 ppm or 0.03 ppm. The change of the pH in the water was also shown to not affect the results substantially (16). This study shows that the control of the acidity of the water is not as crucial as to the control of the impurities in the water. As the crack growth rate of the specimens is shown to be slightly affected by the change in the pH of the water, the purity of the water has been shown to be of greater importance.

3. System Setup

3.1 Previous system

The previous system for this research was created by a University of Idaho capstone group. The group modified an existing autoclave by attaching a servo-hydraulic load frame. An autoclave is designed to carry out industrial and scientific processes in elevated temperatures and pressures. With this attachment, the system could perform fatigue testing in an aqueous environment with elevated temperature and pressure. The design came with a customized Cortest water loop system to circulate the working fluid. A cooling jacket and control system were also designed and implemented by the team to create a fully functional system.

3.1.1 Autoclave Sealing

For the autoclave to fulfill its purpose, a high level of pressure is needed to be maintained within the system. Multiple attempts were made to achieve this. The first was to use mechanical packing material compacted into the cavity between the autoclave lid and rod. This packing, while pressure and temperature resistant, applied hundreds of pounds of friction to the rod when under motion. As such, this design was quickly altered. The second design was a combination of a cooling jacket and seals. To maintain the pressure, two locations require sealing. One for the connection of the autoclave body to the lid, and one to separate the autoclave and cooling jacket fluids. The former is a metal seal with a surface to surface connection. This seal can be seen within Figure 3.1 below. This angled disk is slid around the support columns of the autoclave inside to align with base of the lid. The autoclave itself has a turned down section and is angled to match the seal above it. The lid is then lowered down into the chamber.



Figure 3.1: Autoclave Metal Ring Seal

Twelve 3/4"-16 x 2.5" SHCS (socket head cap screw) are used to tighten down the lid onto the body. This clamping force secures the seal firmly against the machined face and seals the autoclave. As well as sealing in pressure, this seal was fully capable of handling the temperature requirements of the tests. Elevated temperatures up to 300°C were often used during testing so all subsequent seals would have to cope with this condition. As the lower seal was a metallic one, this temperature profile was insignificant as it is under the melting point of the metal.

The secondary method for sealing the autoclave comprised of a pair of rubber u-cup seals. These seals were situated around a pre-designed cooling jacket. One would be used to seal against the high-pressure environment contained within the autoclave itself, while the second would seal the cooling water from escaping out the top of the jacket. Each seal can be seen in Figure 3.2.



Figure 3.2: Original Seals Used in the Cooling Jacket

Due to the need for only one of the pairing to secure against a high-pressure environment, two individual seals were selected. The top seal can sustain only around 7 bar (100 psi, above on the left), while the lower could sustain up to 140 bar (2000 psi, above on the right). Each seal had a melting temperature of ~100°C leading to the need of a cooling system for the seals while under elevated temperature testing.

3.1.2 Cooling Jacket

To combat the heat exiting out of the system and into the seals and cooling rod, a cooling jacket was designed to fit on top of the autoclave. This is a closed system separate from the autoclave. It is a hollow metal shell with an inlet and outlet for the cooling water to flow. The flow of the water touches the seal and is meant to reduce the heat on the seal

due to the convection of the moving water. The jacket in its entirety can be seen in Figure 3.3.

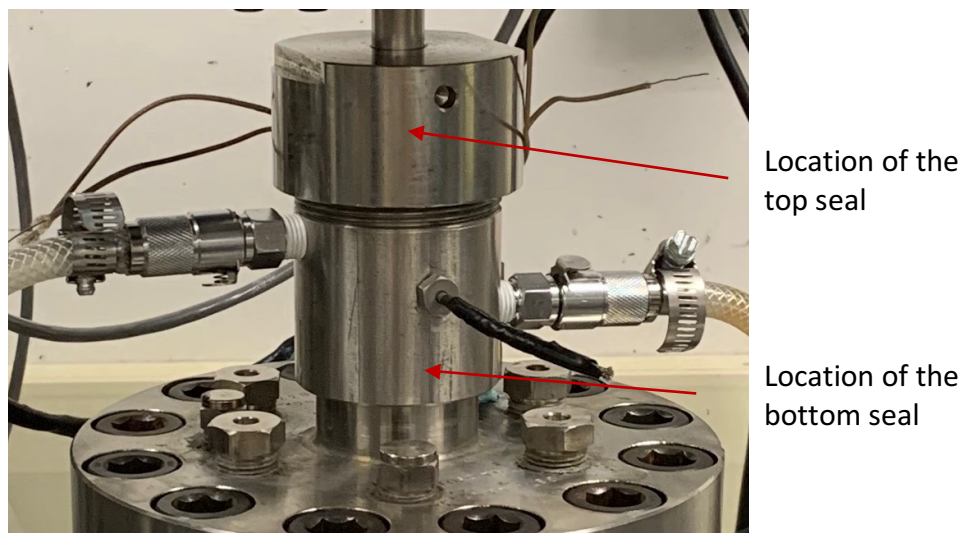


Figure 3.3: Original Cooling Jacket with Water Line Connections

Two quick connect clamps were used to secure the water flow to the jacket. These lines fed in city water at room temperature (RT) to the system. This water would then flow out of the cooling jacket and into the cooling lines of the autoclave closed water loop to further use the water before it went into the outgoing water line. The cooling jacket would sit upon the lower high-pressure seal and compress it when the four tensioning screws were affixed into the jacket top. The top seal would sit inside the jacket upper cavity and be secured by the cap of the cooling jacket when tightened down. In theory, this system would seal against both the pressure from the autoclave and incoming water supply. Originally the cooling jacket was designed to cool the rod so the connected load cell would not overheat. As the test ran, the cooling water would maintain a lower temperature around the rod. The lower seal was believed to be sufficient for the temperature conditions directly underneath the cooling jacket.

3.1.3 Control System

Originally, the intent to control the entire system was through a LabVIEW program ran through a central computer. All subsystems would feed current running information into the program for analysis or safety monitoring. The user would be able to input the

force value and rate of oscillation for the pneumatics to operate. The operating pressures and temperatures would also be able to be altered in this display allowing total control on one device.

3.1.4 Closed Water Loop

Several components of the load frame were purchased directly through Cortest. As well as supplying the chamber and stand, a custom closed circuit water loop was provided. This system comes with water filtration system, heating, and cooling elements. The connection pipes, pump, reservoir, and oxidation management system had not yet been installed. Upon completion of assembly, it would serve as the future fluid management device for the autoclave testing chamber.

3.2 Improvements/Changes

After initial inspection and analysis of the system, changes were necessary. Multiple iterations occurred in the improvement of several autoclave subsystems.

3.2.1 Connection of the Water Loop System

Initially the CWL (closed water loop) from Cortest came unattached from the autoclave system and required several finishing touches to complete the device. The first step was the instillation of the Vision 120 high-pressure pump as seen in Figure 3.4. This pump is capable of supplying 300ml/min of water at 170 bars when at room temp. At maximum temperature, 166ml/min of water at 170 bars is the peak rate. This pump was slotted into the proper receptacle in the display panel and the assembly hoses were coupled with the inlets of the pump's water tank and the outlet to the flow network.



Figure 3.4: High Pressure Pump Used by the CWL

The second action was to attach and seal the water reservoir on the outside of the CWL panel. This 6-foot tall, 7L volume, glass tube serves as the receptacle of the depressurized water waiting to flow from the filters into the pump and back through the system. This tube was fitted with a rubber gasket on both ends and securely bolted into position. This can be seen in Figure 3.5. Securing the tube to the fittings with the rubber gaskets sealed the cylinder and allowed for an internal pressure to be applied creating back pressure on the water producing a smoother flow of the fluid out of this receptacle.



Figure 3.5: Water Reservoir for CWL

Once the CWL was fully functional it needed to be combined with the autoclave. One of the first steps in connecting the two systems was routing several feet of 316 stainless steel tubing to the inlets and outlets of both systems. Once the final location of the autoclave framework was established in the laboratory, the piping was bent and cut to the desired lengths before inserting into the appropriate connections. Once the flow loop was created the cooling water system also needed to be routed. Originally, the cooling system was connected using two ¼" plastic tubes from the two cooling rods on the side of the CWL panel. These were routed from the outlet of the water jacket and out of the cooling towers and into the city water flow outlet.

After the interworkings of the two systems were finalized, the system valve grid would have to be altered to perform the appropriate pumping style. Two different flow designs were possible with the panels valve settings. A "closed" loop system was one such possible configuration in which the autoclave as well as the heating and cooling systems of the CWL could be bypassed and flow would be direct from the pump and into the internal tubing network. This flow path was designed to allow testing of the pump and pressurization of the systems not connected to the autoclave. When flowing, the pump could apply pressure and test the flow throughout the tubing and filtration subsystems. The secondary flow path available was routing fluid from the pump into the heating loop and through to the autoclave chamber. This path incorporated the cooling towers and regenerative heating cycle as well. It would then flow into the filtration system and back into the reservoir for future use. Figure 3.6 shows the two individual presentations of the flow paths respectively as mentioned.

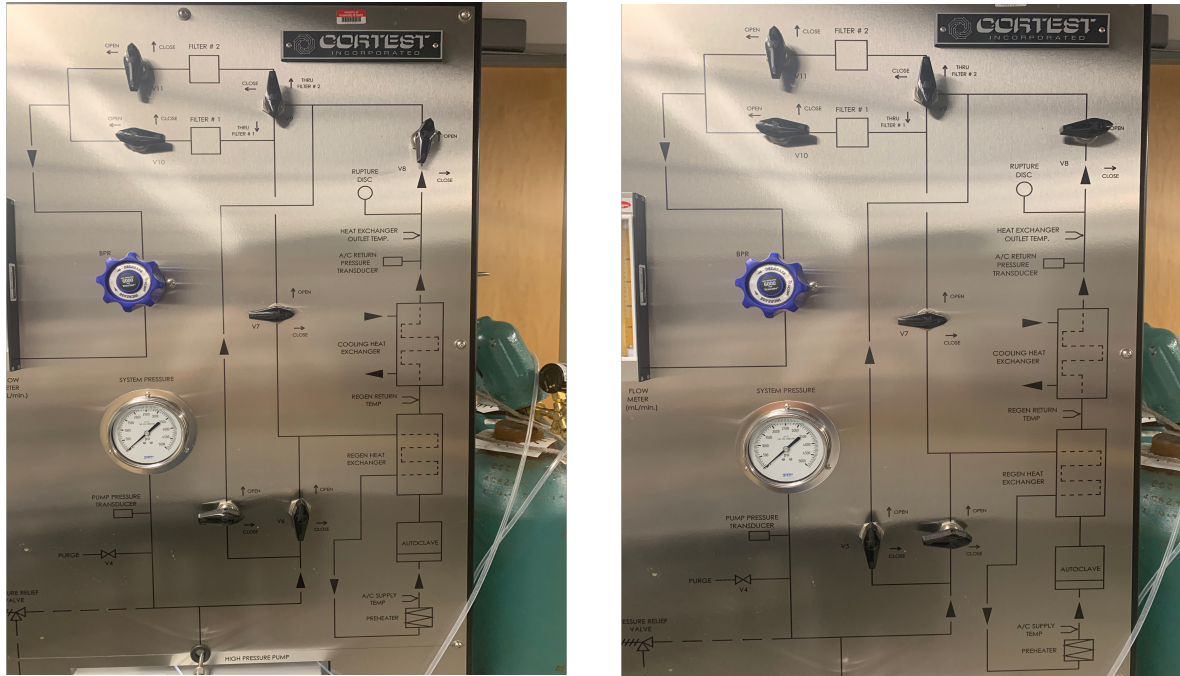


Figure 3.6: Orientation of Flow Valves to Operate CWL

The final step in completing the CWL portion was the addition of argon gas to the reserve water cylinder. This argon gas when bubbled into the water combines with the O_2 particles in the purified water. When coupled, these particles float to the surface and enter the air bubble above the water. This increases the purity of the water and reduces corrosive effects it applies while in the testing chamber. To combine this argon system with the CWL, an argon gas tank was fitted with a gas regulator outlet. This regulator withheld the 200 bar from the tank and released a steady 1-2 bar stream of argon through a plastic tube into the reservoir. Attached at the bottom of the reservoir was a bubbler that evenly and consistently released bubbles of this flowing gas which trap the O_2 particles when opened.

3.2.2 Cooling Jacket

The original cooling jacket designed by the previous group was used in the initial testing of the system. While this system did produce cooling of the load rod, several problems were experienced when full testing was underway. During a FCG test at $288^{\circ}C$ and 85 bar, the lower of the two seals used in this system melted under the high

temperature and ruptured. This resulted in the release of pressure from the autoclave chamber, as well as the heated water inside. When released from this environment, the water instantly vaporized turning into steam as the pressure needed to keep 288°C water in the liquid state is above 70 bar. The upper chamber of the cooling jacket was flowing at about 3 bar, far below that of the autoclave. As well as vaporizing and filling this jacket cavity with steam, it instantly pressurized it with the escaping gasses. As the jacket water line connections are only rated for about 7 bar this caused a rupture of the connection and subsequently blew the lines off their respective quick connects. Although not initially evident, once the pressure and heat had finally been released the seal was found to have been melted. This can be seen later in Figure 3.7. The original design of the cooling jacket had it sitting atop the bottom seal while it was effectively sandwiched between top of the autoclave lid and the cooling jacket bottom. This design meant that the only cooling the seal saw was the top surface touching the metal exterior of the jacket which was being slightly cooled by the convection of the water. Evidently, this was not enough cooling to maintain a safe system and needed to be changed.



Figure 3.7: Failed High Pressure Seal

The first step was the redesign of the cooling jacket and subsequent way of extracting heat away from the seal. Many ideas were submitted and drawn out, but one design was selected and proceeded for testing. Instead of producing a metal shell to flow

cooling water through it, a cooling column was created with an inlet at the top to which the seal would be seated. This column would slide around the rod and be bolted to the top of the autoclave lid. When affixed a coil of wrapped copper tubing was positioned around this tower producing cooling as this coil would conduct the heat away rapidly as the water flowed through the device. The design of the new cooling tower can be seen within the appendices in the associated drawing package.

Aluminum was chosen as the jacket material as its high thermal conductivity is much greater than that of stainless steel which is the material used for the autoclave construction. After turning down a 2" piece of stock and drilling the necessary holes for connections bolts, a cap was created that would properly compress the seal chosen for the new design. Once the jacket was created the copper cooling coil was next. Copper tubing was tightly wrapped around a piece of stock for a total coil height of 5". This was the maximum height possible with the current geometry of the load frame assembly. When the cooling tower was bolted down onto the autoclave, the coil was slid on and connected to the water lines. This new design can be seen within Figure 3.8.



Figure 3.8: Cooling Jacket with Coils Attached

Subsequent testing was then done to ascertain the extent of the cooling produced by this new system. The autoclave chamber heaters were turned on and set to 288°C. Multiple temperature probes were used to analyze how well the heat was being conducted away. During this testing, the working fluid in the chamber was air and no pressure was being applied. Testing of the coils yielded this graph depicting the heat being experienced at each segment of the jacket as seen in Figure 3.9.

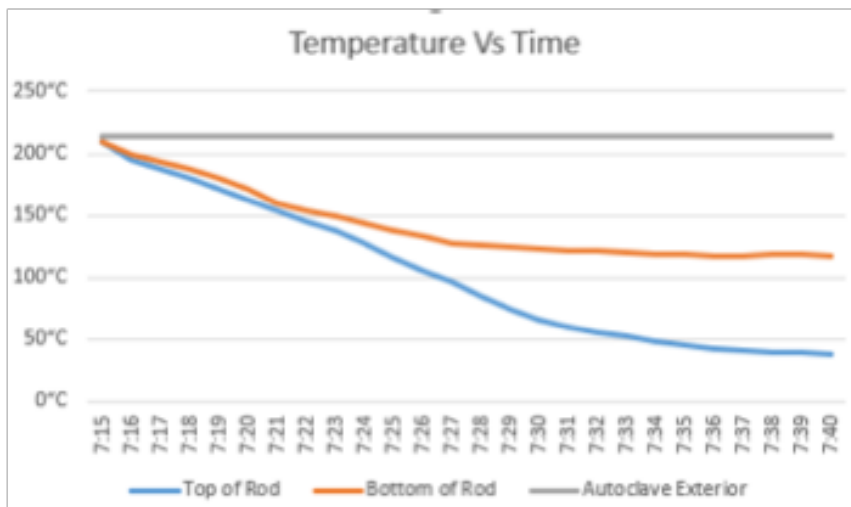


Figure 3.9 Temperature Profiles During Cooling Jacket Testing

As the seal sat upon the upper section of the rod depicted by the blue line, the temperature during testing was seen to be far below the melting temperature of the seal material (~100C). Using this graph and the knowledge of the capabilities of the new seals being inspected, it was assumed that this cooling jacket would be sufficient to sustain the full length of the 85 bar and 288°C test with water as the working fluid.

3.2.3 Seals

As stated above, the previous seal type was found not to be able to cope with the demands of the system at maximum temperature. While a new cooling jacket was designed to improve the conditions for the seal, more improved sealing options were considered. Two features were sought after in the possible new seals. Improved temperature resistance and rupture safety. The latter of which could be attained in multiple different ways depending on the unique design of each seal type. One attractive such seal was one designed by Garlock Sealing Technologies. The design of the seal is made

up of three sections. The first is the male bottom piece made to fit into the recess of the section above. The second section being individual v-rings which are what seal the system. Each ring shares the same geometry allowing for multiple rings to be stacked. On top of these rings is the female section with a reverse geometry of the male allowing for the v-rings to be captured by these two pieces and compressed effectively when inserted into the system. The v-rings multiple layers do not increase the maximum pressure capable of the seal, but rather add safety assurances providing multiple seals in place in case of failure by one of the lower rings.

Once selected for the high-pressure capabilities and the safety feature of multiple seals, one each of the male and female ends were purchased. Four v-rings were selected to fit within the two ends. The heights of the male and female ends were 0.063" and 0.25" respectively. Each v-ring has a height of 0.109". Given the four v-rings applied in this set the total height of the system was measured to be .749" or about $\frac{3}{4}$ ". As noted from Garlock, a compression ratio of 6% was commonly used by their facilities to ensure proper sealing. Given the approximate size of 0.75" for the height of the seal set, the cap extruded end was machined for a height of 0.17". This gave an adequate compression amount of 0.045" or about 6% of the total seal set height when the seals were contained within the cooling jacket cavity. This whole assembly was inserted into the cooling jacket and compressed down with the jacket cap. This set can be seen within Figure 3.10. With this in place, initial testing was in order.



Figure 3.10: V-Ring Seal Set

The first test was to supply water flow through the system. When the chamber was filled with water there was no noticeable leakage from the jacket. When under minimal pressure of about 7 bar leakage was noticed in between the cap and jacket top where the seal was located. Increasing the pressure resulted in more flow out of seal. When inspected the seal was indeed leaking from the seal edge to the jacket. To increase the sealing ability of these v-rings, aluminum sheet metal shims were created with a thickness 0.010". The addition of one shim increased the compression ratio by 1.33%. This increased compression would apply more force to the female portion of the set. Systemically testing the system pressure with increased shims resulted in the following table.

# of Shims	Maximum Pressure Maintained
1	10 bar
2	17 bar
3	28 bar
4	35 bar
5	35 bar

Table 3.1: V-Ring Seal Set Additional Compression Testing

The seal set while providing attractive safety facets, did not maintain adequate pressure without leaking. This result would be compounded under higher temperatures as well. To allow for testing to continue, the previously used high pressure seal was incorporated into the new cooling jacket instead. This seal, while having a lower melting temperature than the V-Ring set, would maintain the pressure for the new design. Based upon previous testing it was shown to be able to withstand the maximum pressures needed. A spacer was introduced to fill the void left by the thinner seal. This seal was then compressed when the cap was attached to the cooling jacket providing the sealing needed.

3.2.4 DCPD Wire Ports

Being a pressurized system, a unique solution was required to attach and utilize the current DCPD (direct current potential drop) wire setup. DCPD is a common method for

monitoring crack growth in FCG testing. ASTM E-647 outlines the use of Electric Potential Difference or EPD to monitor crack length (17). Normally the wires are routed into the heating chamber on a frame to record the data. In this case, they would need to be channeled into the chamber without releasing any pressure or fluid. Specialized wire ports were selected that would allow access to the chamber while under full pressure. Spectite WFS series wire ports were selected to perform this task. Figure 3.11 shows the design of the metal ports and how the wires flow through. Once the wires are inserted into the three plastic rings, the top and bottom sections are threaded together compressing the rings together. This clamping force squeezes the plastic against the wires and molds itself to them allowing zero clearance between the wire and the plastic walls. This effectively seals the wires inside the ports while allowing current to be supplied and readings to be collected by the electronic components.

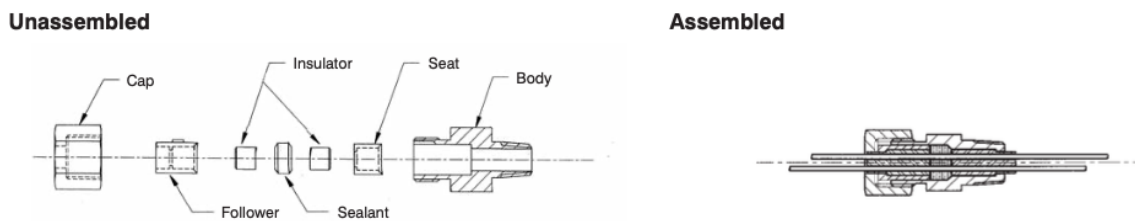


Figure 3.11: WFS Wire Ports Schematics

Four total wires were needed for the current setup. Two are attached to the power supply which administers the constant current to the specimen. The secondary pair is connected to the nanovoltmeter to measure the crack length as a function of voltage. As these wires are different sizes two different ports were needed. The Spectite WFS-1/4"NPT-0.6mm-4-T-A and WFS-1/2"(3/8"NPT)-0.9mm-4-T-A were used for the specific wire sizes. Each having the same function and build geometry, but with different dimensions. To attach these devices, two unused autoclave lid port caps were removed. The two respective wire ports were secured into the lid and sealed with a high temperature thread sealant. A proper length wire for each of the two ports were cut and inserted into the chamber through these ports. As each Spectite WFS port can handle up to four wires at a time, two wire port holes were still open on each device. To fully seal the system four additional small lengths of scrap wire were inserted and compressed with the main wires

to seal the port entirely. Fully clamped down and sealed, the ports were capable of handling pressures up to 140 bar and temperatures above 300°C.

3.2.5 Fluid Controls

Once the CWL was removed from the autoclave system to run the final tests, a new way to add purified water and control the pressure was needed. The CWL inlet and outlet fluid handles were shut and fully closed to deny flow in and out of the autoclave chamber. To ensure full valve closure and stop flow to and from the autoclave, the valve ports V5, V6, V7, and V8 were closed as well to ensure fluid remained in the chamber when under pressure. The autoclave chamber was equipped with a drain valve through a small exit hole in the chamber bottom. This drain valve was used to remove fluid in the chamber. When this drain valve was open, it permitted a clear flow out of the chamber. This also allowed, when connected to a small pump, reverse flow into the chamber. This port was used to flow new water for testing while the chamber was sealed and other flow outlets were closed.

To perform in a FCG test in water above boiling temperatures, changes had to be made to the system. With the CWL removed from the autoclave and fluid now able to flow smoothly in and out of the system, a new method to pressurize the system was needed. For testing, a relatively small amount of pressure was needed to ensure water saturation at lower temperatures. To apply this pressure, another autoclave lid port cap was removed. A brass piping system was attached to an inline pressure gauge. The top of the fixture was fitted with a coupling to which an air compressor hose could be attached. The air compressor supplied the pressure necessary and was checked by the inline gauge. With these alterations in place purified water could be introduced into the system and heated to 150°C while a pressure of 7 bar was applied to maintain the saturation of the water while the test was underway. Figure 3.12 shows the brass fixture used for this purpose.

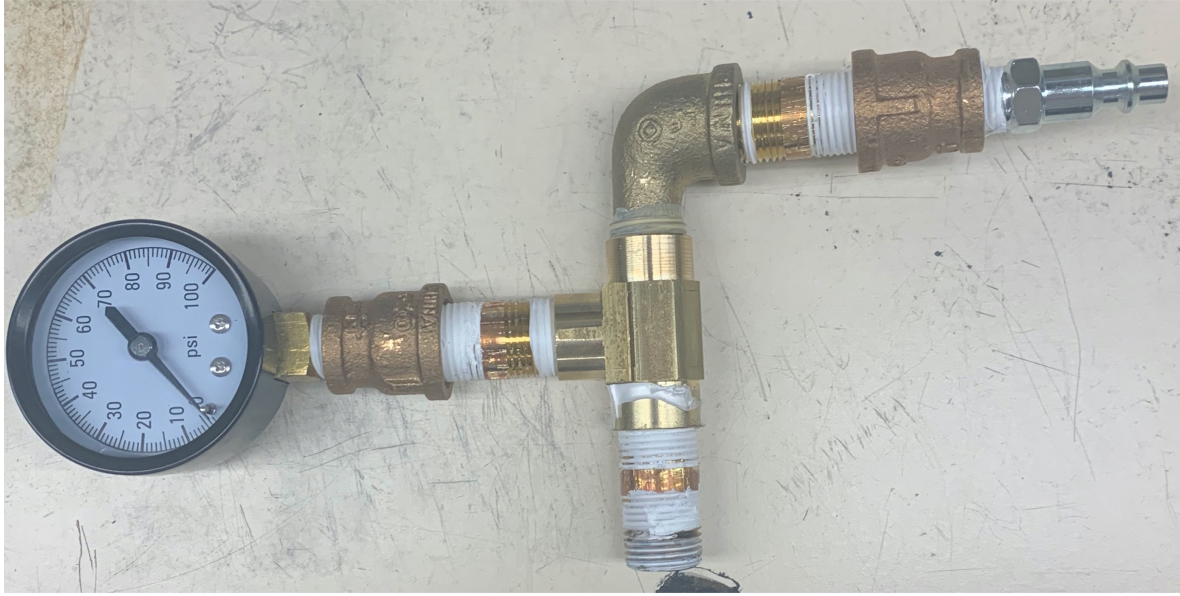


Figure 3.12: Air Compressor and Gauge Attachment

3.2.6 Controls and Data Recording

The overall LabVIEW program designed to control the whole system never came to fruition. A MTS 458.20 MicroConsole controller was used and connected to the load cell and configured for both displacement and load control. A sine wave function was programmed into the controller to perform the FCG tests at a desired frequency. To monitor the internal temperature a two part Cortest temperature controller and monitor was used. The controller lead was connected to the ceramic heater attached to the outer autoclave wall and would heat the autoclave and subsequently the fluid inside. A probe routed into the bottom of the autoclave was exposed to the environment inside the chamber. This probe measured the fluid temperature. These devices were used to ensure a constant and accurate temperature inside the chamber and can be seen in Figure 3.13.

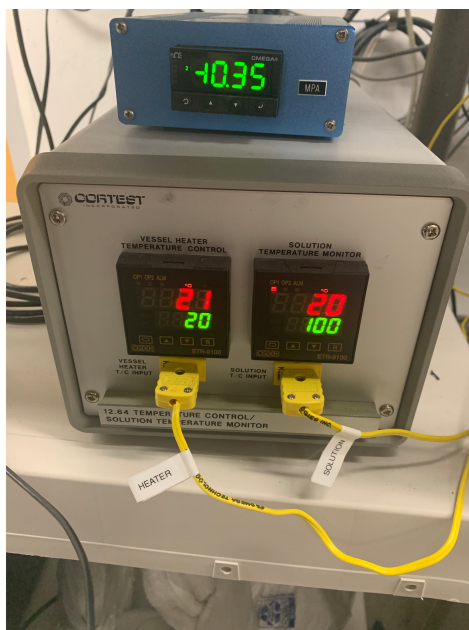


Figure 3.13: Temperature Controller and Monitor

Once the test was underway, the DCPD output needed to be recorded. A LabVIEW program was structured to record each measurement of the device on a set frequency. The program in its entirety can be seen in the appendices. Since the FCG tests were performed under constant frequency, a similar frequency could be used to record data accurately and consistently throughout the duration of the test. The program would record only the voltage value associated with the crack length captured from the DCPD equipment. This voltage would later be paired with a cycle count value during further analysis giving the two data columns needed to perform crack growth rate analysis.

3.2.7 Gaskets

One of the final steps of making the autoclave a fully sealed and water-tight system was the incorporation of two gaskets. The first step was to address the connection between the cooling jacket base and the portion of the autoclave lid it is fastened to. The connection between these two surfaces experiences zero cooling and would need to withstand the full pressure and temperature of the testing environment. A high-temperature extreme-pressure graphite gasket was selected for this purpose. The gasket is rated at 350 bar and a temperature range of -250° to 450° C. The drawing sheet and the dimensions for this disk can be found in the appendices. Holes fitting the bolt pattern of

the cooling jacket base were punched from the graphite. When fitted between the two surfaces and compressed, the disk sealed the gap. Testing up to 100 bar and 300°C yielded no leaks in this section. Figure 3.14 shows this gasket in place.



Figure 3.14: Lower Gasket Attached to Cooling Jacket

The second of the two gaskets was needed to seal the autoclave lid bottom to the chamber top. As seen within Figure 3.15, damage was sustained during one of many openings and closings of the lid by a DCPD wire accidentally being compressed between the seal edges creating a path for fluid to escape the chamber along the original angled metal seal. Another high-temperature extreme-pressure graphite gasket was used to seal this edge as well. A smaller profile was cut from the supplied disk and placed between these two surfaces. The reduction of the disk was to restrict the size enough to not interfere with the autoclave lid bolts while still covering the entirety of the original metal seal area. Once clamped down by the lid when the bolts were secured the gasket was tested thoroughly. Testing up to 100 bar and a temperature of 288°C showed no leakage. The drawing sheet for this disk can be seen within appendices.



Figure 3.15: Damage to Autoclave Metal Seal

4. Experimental Details

4.1 Material and Specimen Details

The material used for the evaluation of this testing assembly was Alloy 709; a solution heat treated austenitic stainless steel with nominal composition of Fe-25Ni-20Cr. Alloy 709 was hot rolled then solution annealed at 1100°C. This resulted in equally dispersed precipitates throughout the microstructure. The composition of the batch can be seen in Table 4.1.

	C	Mn	Si	P	Cr	Ni	Mo	N	Pb	Ti	Cu	Co	Al	Be
Batch #3 Heat 5877-4	0.07	0.91	0.44	0.014	19.93	24.98	1.51	0.148	0.26	0.04	0.06	0.02	0.02	0.0045

Table 4.1: Material Composition by % Mass

Specimens were machined from as-received plates such that the rolling direction was parallel to the crack plane. All specimens used during testing were aged after arrival. Aging of the metal occurred during a six-month period spent inside a furnace at 650°C. This augmented aging time is meant to simulate 50 years in service at 550°C which is common reactor water temperatures. Aging to this stage in a component is referred to as, Aged 2, where Aged 1 would be simulating 25 years of service at 3 months inside the furnace. All specimens used during this research were Aged 2. These specimens were used as part of a previous research effort and were available to be used as specimens in this process.

The specimen geometry for FCG testing was the standard C(T) geometry, outlined in ASTM E-647 (7). Important measurements include the width, thickness, and notch length. Since all tests performed were FCG tests, no side grooves were introduced which is common in CFCG tests. The notch and details were machined using wire electrical discharge machining (EDM) in accordance with ASTM standards for the C(T) geometry. All other features of the specimens were machined on a CNC mill. A schematic drawing of the

specimen can be seen in Figure 4.1. All dimensions were defined in accordance with ASTM Standard 2760 creep-fatigue crack growth testing (18).

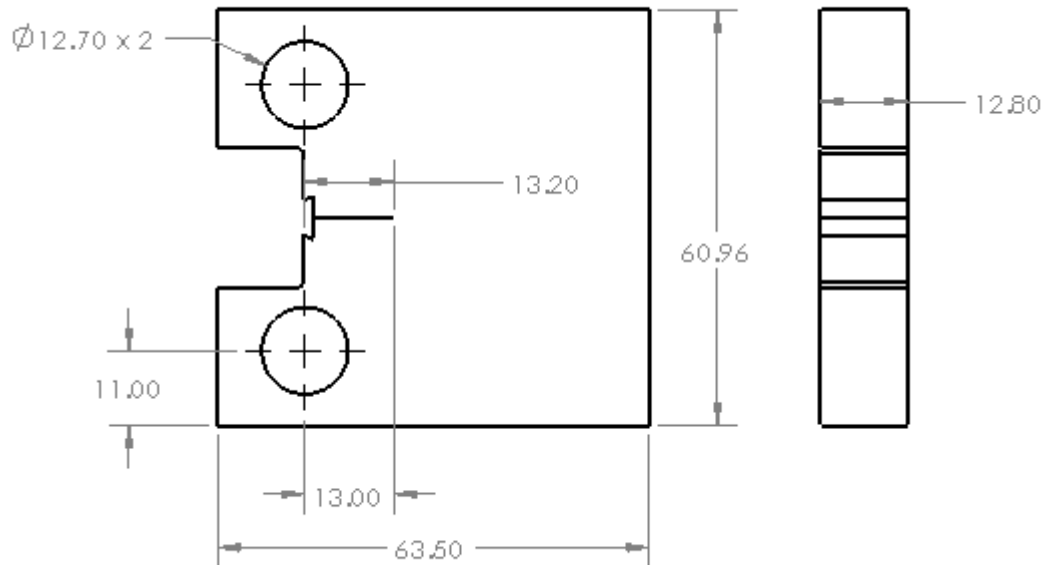


Figure 4.1: C(T) Specimen Dimensions in Accordance with ASTM E-647

4.2 Experimental Procedure

The procedure of performing the FCG tests include three main steps. These include precracking, DCPD wire setup, and the separation of the two specimen halves for surface analysis.

4.2.1 Precracking

The first step was precracking a specimen from the notch length of 13.2 mm to a total crack length of 18mm. This established the initial crack length, or a_0 for the remainder of the FCG test. This crack length was established in accordance with ASTM E-647 as above 10% of the specimen thickness (7). All precracking was performed at room temperature and a frequency of 15 Hz. The MTS TestStar computer and associated load frame utilized a built in FCG software to precrack the specimens. Inputs include specimen notch length, width, thickness, and modulus of elasticity. Final crack length and ΔK were selected as 18 mm and $18 \text{ MPa}\sqrt{\text{m}}$ respectively. The precracking software used load shedding to reach these two values simultaneously while in ΔK control. A maximum

shedding rate, $c = -0.08 \text{ mm}^{-1}$ was used as per ASTM Standard E-647 (7). The software used Equation 7 to calculate the stress intensity to control the load as the system progressed with the cracking.

$$\Delta K_n = \Delta K_0 e^{c(a_n - a_0)} \quad (7)$$

Where ΔK_0 and ΔK_n are the current and proceeding stress intensities respectively as well with the crack lengths a_0 and a_n .

As the software was load shedding the maximum load was approximately 16kN and would subsequently drop to about 9kN once the desired end conditions were met. This would produce an initial K_{max} value of nearly $28 \text{ MPa}\sqrt{\text{m}}$ and would drop to down to approximately $20 \text{ MPa}\sqrt{\text{m}}$. With the applied $R=0.1$ mean stress ratio this would give ΔK values of about $25 \text{ MPa}\sqrt{\text{m}}$ down to $18 \text{ MPa}\sqrt{\text{m}}$ which was the desired starting point for the testing.

4.2.2 DCPD Measurement Technique

DCPD is a common method for monitoring crack growth in FCG testing. In this technique current is routed throughout the specimen and the voltage jump across the crack along the specimen is measured. This voltage is correlated to a crack length and used to obtain a growth rate when compared to the cycle count. Direct current was applied to the specimens through a Keithley 2280S-32-6 DC Power Supply. This precision current power supply delivered a constant current of 2 Amps to the specimen front edges. To measure the voltage jump created, a Keithley 2182A Nanovoltmeter was used. These connection wires were attached on both sides beside the notch line as can be seen in the right side of Figure 4.2. The current supplying wire attachment points were on the front face of the specimen, one above and one below which can be seen in the left side of Figure 4.2. The combination of these two devices produced a resolution of $\pm 2\mu\text{V}$.

To apply and measure using this technique each device had a positive and negative lead current welded to the specimen. Nichrome 60 wires were used for this purpose to prevent corrosion found within the autoclave environment. Applying roughly 20 Amps of

current to the specimen and connecting the wire would solidly weld the wire in place to the specimen exterior. 22-gauge and 26-gauge wire were used for the power supply and the nanovoltmeter respectively. The full wiring diagram can be seen within Figure 4.2.

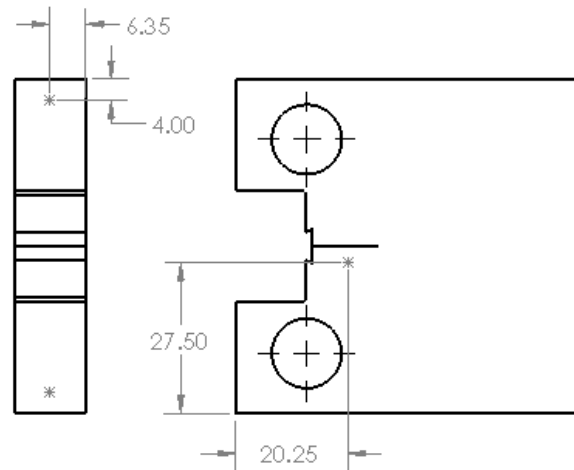


Figure 4.2: C(T) Specimen Wiring Schematic

4.2.3 Setup in Autoclave

Once a precrack was completed and the wires were attached onto the specimen, it could be placed into the autoclave chamber. The autoclave lid structure would be detached from the load cell. Once this was removed, the specimen would be pinned in place to the Inconel grips with two pins through the machined edge holes. The rod, when attached to the load cell, extends too far to successfully affix the specimen while the chamber and lid are together. The wire leads connected to the specimen are wrapped together with the ends of the wires routed through the ports on top of the lid. The lid with specimen attached would then be rethreaded into the load cell receptacle. The cooling jacket and lower lid seal would then be placed atop the lid before lowering it into place and tightening the 12 screws to secure the system. The wire port leads were then connected to the ends of the two DCPD measurement devices.

Once the specimen was in place, the chamber environment could be established. Filling the chamber with the purified water was the first step. The chamber ceramic heating wrap was then turned on and set to the desired temperatures. Simultaneously, the

pressure inside the chamber was introduced and increased to reach a point above the water saturation pressure for the test. With the appropriate pressure and temperature now in place, the fatigue testing could begin. A sinusoidal waveform was used during the testing. Increasing the set point and span on the load control module applied an $R = 0.1$ ratio of approximately 9000 to 900 N (2000-200 lbs). The test is continued until the crack length reached a critical value related to the life of the specimen.

4.2.4 Breaking the Specimen

Once the specimen had reached an adequate crack length, the specimen was removed from the autoclave. At RT, the specimen was slowly pulled apart until halves of the specimen were created. These were then used for later data analysis.

4.3 Data Collection

To collect FCG data during the test a LabVIEW program was created to record the DCPD values. Afterwards, Matlab was used to analyze this data and compute crack growth rates as well as stress intensities for each data set. Physical crack length values were then taken as a check from the surface of the specimen. These values were then used to offset the acquired DCPD values.

4.3.1 Software Analytics

A program to capture the DCPD nanovoltmeter readout was created using LabVIEW. The recorded data was transferred to a segmented text file where it could be analyzed later. The program used can be seen in the appendices. From this voltage value a crack length is calculated in Matlab. This DCPD data is then paired with individual cycle count data. Taking the difference between the data points creates crack growth rates which can then be plotted and further analyzed. This reduction and analysis code can be seen within the appendices.

4.3.2 Microscopy

To ensure the accuracy of the DCPD values, the surface of the crack line was inspected for the physical lengths of each important region. The beginning of the notch, precrack, and final crack profile were inspected and measured under a microscope. Taking 5-6 points across the crack front provided an average crack length for the region. Figure 4.3 shows the surface of a fragmented specimen as well as the crack line from which points were taken. These physical crack lengths shown were used as offsets for the data reduction. The transition from the end of the test to the point at where the specimen is fractured is evident from the discoloration due to the lack of applied temperature. This allows for a clean line to be deciphered while under a microscope.

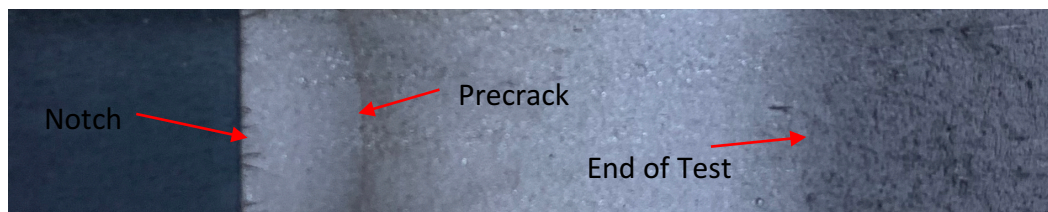


Figure 4.3: Broken Specimen Surface and Critical Crack Length Positions

5. Results

5.1 Comparing Autoclave to Additional Load Frames

The first test of the autoclave's capabilities was to replicate simple fatigue testing operations of the other hydraulic frames. Once the load cell framework and data collection equipment was fully attached a FCG test was ran in the autoclave. This test was performed at 288°C in air. This was the desired maximum temperature to achieve in the autoclave later in an aqueous setting. As standard during this research the test was performed at a stress ratio of $R = 0.1$ with a load range of 9000-900 N. This test would serve as the baseline to compare the abilities of the autoclave setup to the alternative load frames. Both specimens were precracked to the same starting ΔK of $18 \text{ MPa}\sqrt{\text{m}}$ and a crack length of 18mm. The two tests and the crack growth results can be seen in Figure 5.1.

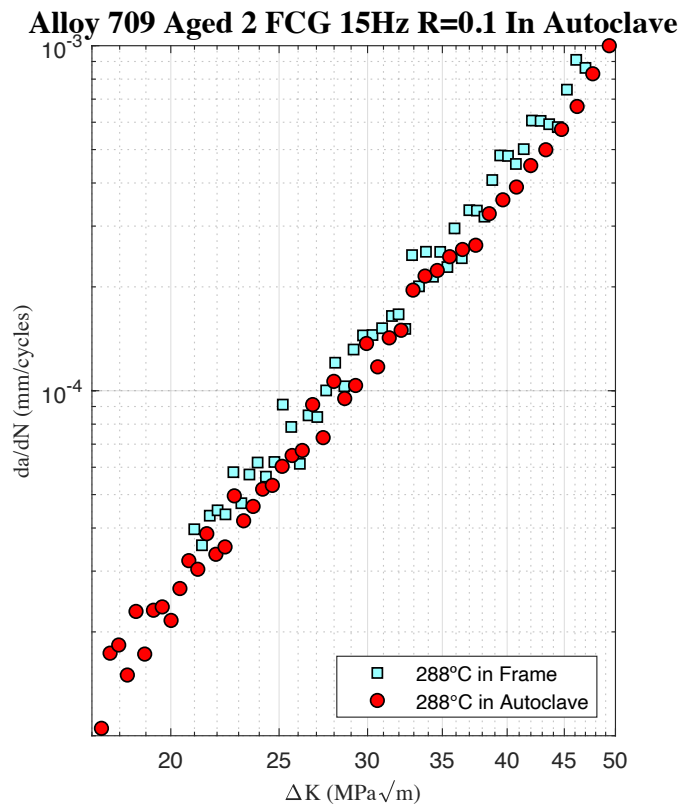


Figure 5.1: FCG Test Data Comparison Between the Original Load Frame and the Autoclave

The tests compare well until the higher end of the of the stress intensity range when there is a slight divergence. The deviation between the two sets of data was 5% at maximum. A Δa of .2mm was used to analyze all points as per ASTM standard E-647 for crack growth data collection rates (7). This Δa interval was used for each test for da/dN and ΔK . Increased scatter was recorded at lower ΔK values because the stress intensity equation changes very little with small Δa increases.

As seen above the results were very similar and showed the success of the autoclave load cell setup. Minor differences in data point correlation can be attributed to averaging within the data reduction process. As the test involves hundreds of thousands of cycles, numerous data points are recorded and can be averaged together to form numerous similar points. The noise experienced within each test by the DCPD equipment will always lend to small differences, but the crack growth rates of these two tests were very similar.

5.2 Data Collection in Pure Water

Once testing of the autoclave functions were validated, testing in water as the working fluid was commenced. Gathering data within an aqueous environment had not been completed before, so the first test was one in purified water in room temperature and atmospheric pressure. A FCG test was administered to another specimen on the additional load frame in room temperature as a baseline to compare against. Once the crack had been growing for about 50000 cycles, water was introduced to the chamber and until the whole internal system was submerged. The resulting graph displays the results of this test.

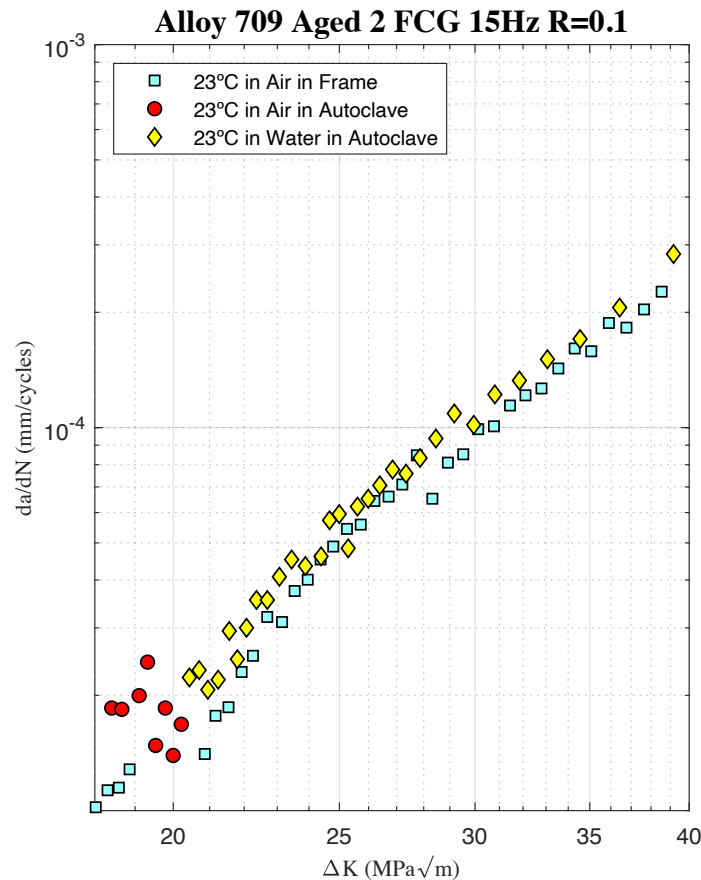


Figure 5.2: RT Comparison of FCG Test in Air and Water

High levels of noise were experienced within the first section of the autoclave test before the water was introduced. Reduction and averaging of the data reduced the spread slightly. A slight upward “jump” in DCPD voltage value occurred when the water first touched the wires connected to the specimen. This jump was then subtracted later in data analysis as the crack had not grown, but the equipment needed more voltage from the power supply to continue generating 2 amps throughout the specimen. This change in wiring voltage subsequently increased the value read on the nanovoltmeter. Once this voltage change was factored out for the test, the results fit well within each other. Above this zone when the water was introduced, the system established a steady crack growth curve with much less noise experienced. This range contained about 5% deviation from the baseline test in the additional load frame. As seen the two tests correlate well. Small

overlap is seen within both data sets. Once again as with previous tests, minor data correlation variation can be assumed by averaging techniques upon the large-scale data points recorded throughout each test.

5.3 Data Collection in Heated and Pressurized Water

As data collection in the aqueous environment had proven successful, the next step was to test with pressure and temperature. Due to the previously stated issues regarding lack of cooling within the cooling jacket and sealing limitations, a lower than maximum condition environment was introduced. A temperature of 150°C was applied to the water inside the chamber. At the same time a pressure of 7 bar (100 psi) was applied to prevent the vaporization of the fluid. A FCG test was performed for the test duration until failure.

While the temperature and pressure were maintained throughout the test, one issue was noticed. The compression of the seal used within the cooling jacket was creating a frictional force that altered the load applied to the specimen. While originally planning for a mean stress ratio of $R = 0.1$ to be applied as in similar tests, a ratio of approximately $R = 0.3$ was performed. The friction reduced the upper load by 25% which produced this stress effect. This shifted the data on the crack growth chart to the left as can be seen within Figure 5.3.

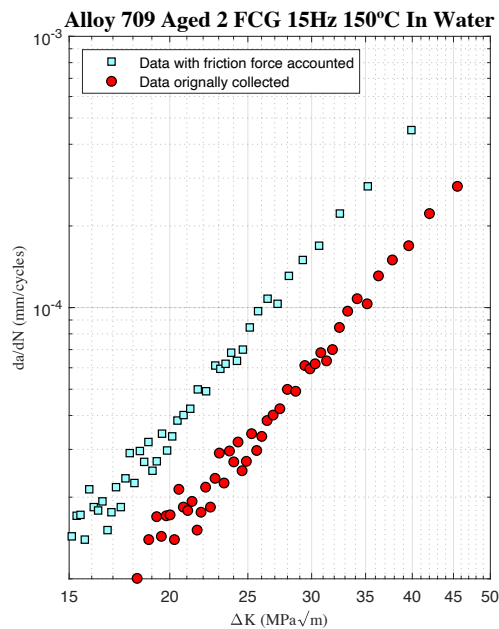


Figure 5.3: Shift Accounting for Frictional Force

This reduced load inadvertently reduced the stress intensity shifting the data to the left while maintaining the crack growth rate.

5.4 Total Test Comparison

Combining all tests shows the progress the autoclave has produced in crack growth data collection over this research. Figure 5.4 shows all tests completed in the autoclave as well as the baseline tests completed within the additional frames for verification.

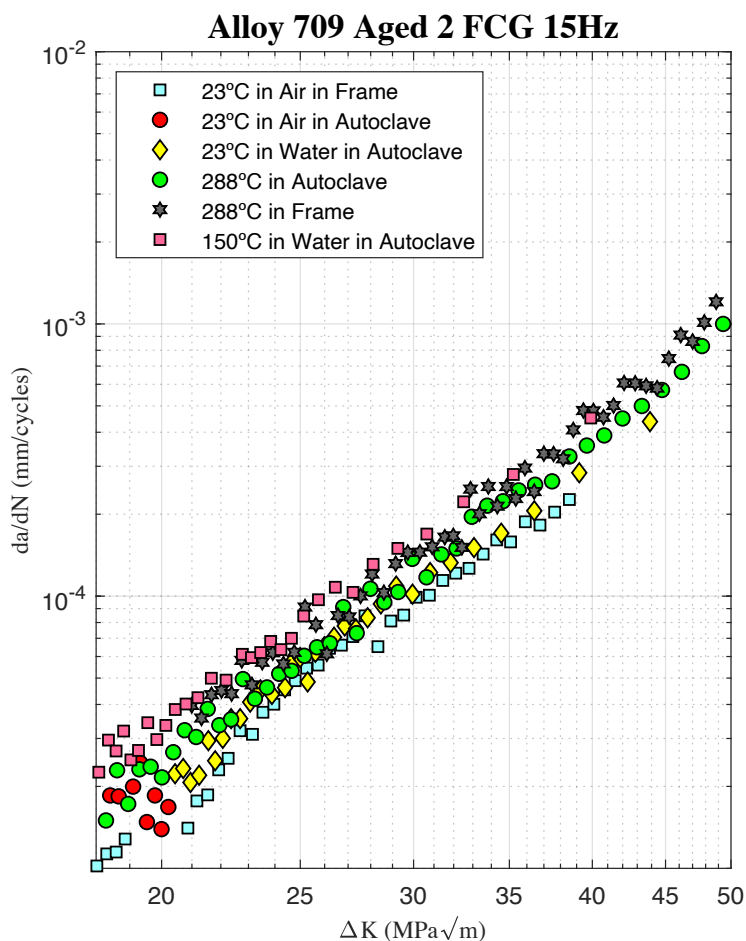


Figure 5.4: All Tests Completed During Research

As seen the crack growth between RT and 288°C is very similar. Slightly faster growth is achieved during these tests, but the results are comparable with those performed at the lower temperature. The test performed in higher than boiling temperature water under pressure was successful, but as seen is shifted from expected positioning between the two temperature tests above and below it. All tests experience noise in the beginning stages of

the tests due to the amount of cycles needed to attain significant growth leading to the spread of data points. As the crack grows, the rate becomes more stable and the noise is reduced considerably leading to more accurate data curves.

6. Conclusions

6.1 Autoclave Fatigue Performance

The autoclave is fully capable of performing crack growth tests like those completed on the additional frames. DCPD data can be collected and analyzed in full for each type of test. FCG and CFCG tests are both capable with the current load cell and monitoring equipment setup. All temperature settings for testing in air are available within the chamber. Sufficient cooling was applied to perform this type of testing. As seen above in chapter five the data variance within the baseline testing was less than 5%. This shows the accuracy and capability of the frame to simulate tests previously performed on other hydraulic frames.

6.2 Collecting DCPD data in Water

Introducing water as the working fluid into the autoclave chamber while collecting DCPD data was shown to work and be successful. With the adequate seals in place the chamber could be closed and filled with the purified water. The DCPD system does experience a “jump” in value when the wires encounter the fluid, due to the need for more power from the DC power supply. This jump can be corrected later in each case as it is a one-time event. Once corrected the test performs just as well as in air for the duration of the test. Crack growth during FCG testing in the two environments did not show any significant variance. The limited time in the corrosive environment does not affect the specimen enough to show any significant results. Fluid in this testing mode can be heated to anything below 100°C before pressure will need to be applied as well as the seals are still capable of maintaining a leak-tight system.

6.3 Collecting DCPD data in above boiling temperature water

The ability to collect DCPD data in above boiling temperature water was proven to be successful. As it was with a zero-internal pressure water test, the specimen showed no

additional effects from the aqueous environment due to the limited time. The heightened temperature increased the crack growth rate slightly above that of the RT tests as expected. The addition of pressure into the environment did not affect the DCPD data collection setup and data was collected successfully as with every other test.

Overall the autoclave's ability to maintain the maximum pressure of 85 bar and 288°C for the duration of a FCG was proven to be unsuccessful. Pressure could be applied up to the maximum value required for testing and maintained. However, the maximum temperature needed could not be sustained. The cooling jacket setup with the several seals tested could not handle the highest temperature desired for testing. At 288°C the seals failed resulting in the release of pressure and vaporized water from the cooling jacket rupture point. This inability to replicate reactor water settings meant a modified test was needed to obtain data in above boiling temperature water. At a lower temperature, the needed pressure to maintain water saturation is considerably lower. The attached air compressor successfully applied enough pressure to measure DCPD data in 150°C water. While failing to meet the ultimate conditions the frames ability to collect and analyze data collected in this heated and pressurized aqueous environment was proven successful. Further alterations to this system are needed to attain the testing results of reactor water settings. As is, the system does not provide enough cooling or have the materials in place to withstand this high temperature.

7. Recommendations

7.1 Sealing and Cooling

The results of this research show the promise of this system in fatigue testing submerged in higher than boiling temperature water. A few key components would need to be improved upon to facilitate the desired testing in the future. One of these improvements to be made is proper sealing around the autoclave lid and cooling jacket sections. The current seals in place for the cooling jacket are only capable of withstanding 100°C temperatures during testing. Ultimately this is not enough and the current system can be modified in several ways to handle higher temperature tests. One is to change the

material the seal is made from. Several rubber material candidates can surpass this original maximum temperature. Siliconic rubber and fluorinated rubber each have a higher stable maximum working temperature of 180°C and 200°C respectively. This substantially raises the amount of heat the seals can receive from the autoclave without failure. Keeping the same seal setup can mitigate the frictional force created by seal sets like the one tested earlier. Custom seals can be made of these materials raising the working temperature and reducing the need for a superior cooling jacket design.

The maximum cooling jacket space is limited to the rod height and current design of the autoclave. This space is already occupied by the current design so extending the jacket and adding more cooling wraps may not be an effective idea to improve the cooling to the seals. One option is adapting the current design to have a cavity included within the cooling jacket as well as maintaining the wraps. The current design works much like a heat sync and draws the heat onto aluminum shell at which point the copper cooling coil wraps extract the heat. The problem is the lack of the usable surface area. If a hollowed chamber was added to the jacket throughout the upper section, more surface area for cooling water to touch would be possible. The diagram in Figure 7.1 shows the possible look of such a system. The coils would be maintained to cool the exterior of the jacket as well providing backup to this system. The jacket with both these sources of cooling would have the exterior and interior cooled much closer to the seal itself decreasing the chance of failure due to the heat.

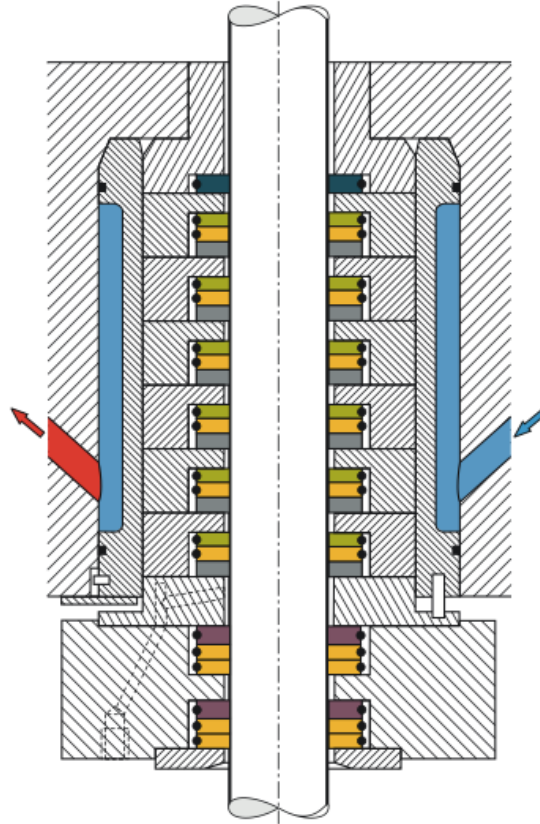


Figure 7.1: Possible Cooling Jacket Modifications

7.2 Notification System

One of the requirements of this assembly is the ability to run SCC tests. These tests often incorporate 600 second or longer hold times and can take weeks and up to months to finally break the specimen. The ability to be away from this frame while tests are running is needed during these extended tests. One safety mechanism needing to be put in place is a notification system for certain system failures. Several places along the system's workings are the most likely sources for failure and therefore could have devices in place to notify the user of this occurrence. The first is the cooling water and jacket sealing area. This area can be equipped with temperature sensors and probes to monitor the value at these sources. If too much heat is applied to the seal for risk of melting or the system fails and steam from the autoclave escapes into the cooling water, the monitors can notify the LabVIEW setup to communicate with the user via direct messaging. Another area of need is the concern of the CWL pump running without water. If a leak somewhere in the system

was to occur and water was to drain out of the system, the reservoir of additional water would eventually run out. This would cause the pump to be running on air which could damage this costly piece of equipment. Flow rate sensors could be added to the line after the integrated cooling section of the CWL. If leakage occurred the sensor would pick up the lack of flow eventually and notify the user of the occurrence. Thirdly, an internal notification system monitoring the DCPD value should be applied. Any major change in system pressure or water quality would alter this value from the nanovoltmeter. A range of acceptable noise could be applied to filter out small changing values. This along with all other systems can be fed into the DAQ and monitored with the LabVIEW system currently running. Programming in a notification system via direct messaging for all these systems is very attainable.

7.3 Maintenance

Damage was sustained throughout the system during the research. Opening and closing the lid of the autoclave has the tendency to catch the DCPD wires hanging from the specimen and squeeze them between the two metal seal surfaces. One gouge during a testing session was created by compressing the wire enough to form a divot that allows fluid to pass and escape the seal. The divot was temporarily fixed by the addition of the larger graphite disk to seal the lid against the pressure. To negate the use of the current graphite disk, the rim would have to be recut and smoothed down on the CNC to ensure the profile is flat once again. With this recut the lid could be lowered and attached without additional gaskets being needed. Another source of damage is the high-pressure valves used on the CWL control panel. These valves use a Teflon lining inside to allow smooth rotation of the ball bearing and control the flow. While being able to withstand high pressure water, the linings cannot be touched by steam. When the seals broke in the original testing and allowed high temperature steam to escape into the CWL, this affected the Teflon linings and caused the ball bearings to not be able to fully seal. These need to be replaced before proper sealing of side channels along the systems pipe network can be performed. Lastly, to maintain the safety and functionality of the electronic equipment in the event of a failure, shielding should be erected around the autoclave exterior to deny

potential steam and water that could escape from touching the electronic equipment and causing damage. This shielding would serve both to protect the equipment as well as the user in the event of another failure like those before.

References

1. "Sodium-Cooled Fast Reactor (SFR) Technology and Safety Overview." *Washington, DC*, 18 Feb. 2015.
2. Evropin, S V, and V M Filatov. "SERVICE-LIFE ANALYSIS OF NUCLEAR REACTOR ELEMENTS UNDER HIGH-FREQUENCY RANDOM LOADING." *Atomic Energy*, vol. 113, ser. 4, Feb. 2013, pp. 258–264. 4.
3. Chengliang, Li, and Yang Mengjia. *The Challenge of Nuclear Reactor Structural Materials for Generation IV Nuclear Energy Systems*. Aug. 2009.
4. Sham, T L, and K Natesan. "Code Qualification Plan for an Advanced Austenitic Stainless Steel, Alloy 709, for Sodium Fast Reactor Structural Applications." *Argonne National Laboratory*.
5. Barsom, John M., and Stanley T. Rolfe. *Fracture and Fatigue Control in Structures: Applications of Fracture Mechanics*. ASTM, 2006.
6. Stephens, R. I., et al. *Metal Fatigue in Engineering*. Wiley, 2001.
7. "ASTM E647-95a: Standard Test Method for Fatigue Crack Growth Testing."
8. Upadhayay, Swathi, et al. "A Study on Tensile Properties of Alloy 709 at Various Temperatures." *Materials Science and Engineering: A*, vol. 733, 2018, pp. 338–349.
9. Rabiei, Afsaneh, et al. "Creep and Creep-Fatigue Crack Growth Mechanisms in Alloy709 — NEUPRC-3.2 (Final Report)." 2019.
10. Shaber, Nicholas. "Investigation of Fatigue and Creep-Fatigue Crack Growth in Alloy 709 at Elevated Temperatures." Dec. 2018.
11. Potirniche, Gabriel, et al. "Characterization of Creep-Fatigue Crack Growth in Alloy 709 and Prediction of Service Lives in Nuclear Reactor Components (Final Report)." 2019.
12. Alomari, Abdullah S., et al. "Creep Behavior and Microstructural Evolution of a Fe-20Cr-25Ni (Mass Percent) Austenitic Stainless Steel (Alloy 709) at Elevated Temperatures." *Metallurgical and Materials Transactions A*, vol. 50, no. 2, 2018, pp. 641–654.
13. Andresen, Peter L. "Stress Corrosion Cracking of Current Structural Materials in Commercial Nuclear Power Plants." *Corrosion*, vol. 69, no. 10, 2013, pp. 1024–1038.
14. Andresen, P. L., et al. "Effects of Hydrogen on Stress Corrosion Crack Growth Rate of Nickel Alloys in High-Temperature Water." *Corrosion*, vol. 64, no. 9, 2008, pp. 707–720.
15. Andresen, P. L. "Emerging Issues and Fundamental Processes in Environmental Cracking in Hot Water." *Corrosion*, vol. 64, no. 5, 2008, pp. 439–464.
16. Was, G. S., and P. L. Andresen. "Stress Corrosion Cracking Behavior of Alloys in Aggressive Nuclear Reactor Core Environments." *Corrosion*, vol. 63, no. 1, 2007, pp. 19–45.
17. "ASTM E647.A3: Guidelines for Electric Potential Difference Determinations of Crack Size."
18. "ASTM E2760-10e2: Standard Test Method for Creep-Fatigue Crack Growth Testing."

Appendices